Three-Dimensional Nearshore Currents Model
Based on Vertical Distribution of Radiation Stress

Hisamichi Nobuoka[1], Nobuo Mimura[2] and Hajime Kato[3]

Abstract

Wave-induced currents in a surf zone must be explained by the change of wave motion. The driving force for nearshore currents is the radiation stresses which are defined as the excess momentum flux due to wave motion. However, there is no model which can describe the three-dimensional structure of the nearshore currents. This study aims to develop a model of this kind, in which only wave motion is taken as the driving force to the currents. Governing equations are derived from the Navier-Stokes equations. This model is proved to reproduce the currents measured in the experiments.

1. Introduction

Nearshore currents in a surf zone have a three-dimensional structure (e.g., Svendsen et al., 1989). They have been dealt with by the combination of horizontal and vertical circulations. The generation of the horizontal circulation has been expressed with radiation stresses averaged over a water depth. On the other hand, it is suggested that the vertical circulation including undertow is caused by the imbalance between the momentum flux of wave motion and pressure force in a vertical plane (Dyhr-Nielsen et al., 1970).

Some models for the vertical circulation including undertow take into account the role of rollers associated with wave breaking. These models are classified into two types. One is an undertow model proposed by Svendsen (1984). The undertow model needs to empirically assume the volume rate of the undertow compensating the onshore

---

[1] Research Associate and [3] Professor, Dept. of Urban & Civil Eng. Faculty of Eng., Ibaraki Univ., Nakanarusawa, Hitachi, Ibaraki, 316, Japan (e-mail hnob@hit.ipc.ibaraki.ac.jp)

[2] Professor, Center for Water Environmental Studies, Ibaraki Univ., Nakanarusawa, Hitachi, Ibaraki, 316, Japan

flux above the wave trough. In a three-dimensional beach, however, the estimation of compensating flow is very difficult, for onshore and offshore flow rates are not necessary balanced in a vertical section. The other type is a model which considers the momentum flux of surface roller as driving force for the vertical circulation. It is not clear, however, how the momentum of surface roller occur.

    This study aims to propose a new type of three-dimensional nearshore currents model on the basis of two concepts; i.e., the flux of onshore flow above the trough level and offshore flow under the trough level themselves are variable to be obtain, and a driving force for currents is only wave motion. At first, governing equations are derived from the Navier-Stokes equation. Then, the mechanism to generate time-mean currents are discussed. The predictive capacity in this model is also examined by comparing the computational results with measurements of cross- and long-shore currents in different settings.

2. Governing Equations and Numerical Solution

    Basic equations to derive the time-mean equations are the Navier-Stokes equations of continuity (Eq. (1)) and momentum conservation (Eq. (2) and (3)).

$$\frac{\partial u}{\partial x} + \frac{\partial w}{\partial z} = 0 \tag{1}$$

$$\frac{\partial u}{\partial t} + \frac{\partial u^2}{\partial x} + \frac{\partial uw}{\partial z} = -\frac{1}{\rho}\frac{\partial p}{\partial x} \tag{2}$$

$$\frac{\partial w}{\partial t} + \frac{\partial uw}{\partial x} + \frac{\partial w^2}{\partial z} = -g - \frac{1}{\rho}\frac{\partial p}{\partial z} \tag{3}$$

where u, w are the total instantaneous fluid particle velocity in the x and z directions, p is pressure, ρ is the mass density and g is gravity. The terms in y direction are similar to the x terms, but are not presented here for the sake of brevity. Furthermore viscous terms are not expressed now as they will be small except in the bottom boundary.

    Equations (1), (2) and (3) are transformed into the Reynolds equations by dividing the velocity components and pressure into three components (Eq. (4)).

$$u = \overline{u} + u_w + u'$$

$$w = \overline{w} + w_w + w'$$

$$p = \overline{p} + p_w + p' \tag{4}$$

where $\bar{u}$, $\bar{w}$, $\bar{p}$ are time-mean components, u_w, w_w, p_w are periodic components associated with wave motion, u', w', p' are turbulent fluctuating components. The time-mean quantities in Eq. (4) satisfy the following relation:

$$\bar{u'}, \bar{w'} = 0$$

$$\bar{u}_w, \bar{w}_w = 0 \text{ (except above trough level)} \tag{5}$$

We obtain Eq. (6), (7) and (8) substituting Eq. (4) to Eq. (1), (2) and (3).

$$\frac{\partial(\bar{u} + u_w + u')}{\partial x} + \frac{\partial(\bar{w} + w_w + w')}{\partial z} = 0 \tag{6}$$

$$\frac{\partial(\bar{u} + u_w + u')}{\partial t} + \frac{\partial(\bar{u} + u_w + u')^2}{\partial x} + \frac{\partial(\bar{u} + u_w + u')(\bar{w} + w_w + w')}{\partial z}$$
$$= -\frac{1}{\rho}\frac{\partial(\bar{p} + p_w + p')}{\partial x} \tag{7}$$

$$\frac{\partial(\bar{w} + w_w + w')}{\partial t} + \frac{\partial(\bar{u} + u_w + u')(\bar{w} + w_w + w')}{\partial x} + \frac{\partial(\bar{w} + w_w + w')^2}{\partial z}$$
$$= -g - \frac{1}{\rho}\frac{\partial(\bar{p} + p_w + p')}{\partial z} \tag{8}$$

The pressure p at arbitrary height z can be calculated after integrating vertical momentum equation (Eq. (8)) between water surface η and z. The following equation is obtained assuming that interaction between the components is not exist (Assumption-1) and that pressure at the water surface is zero.

$$\frac{1}{\rho}(\bar{p} + p_w + p') = g(\bar{\eta} + \eta_w + \eta' - z)$$
$$+ \frac{\partial}{\partial t}\int_z^\eta (\bar{w} + w_w + w')dz$$
$$+ \frac{\partial}{\partial x}\int_z^\eta (\bar{u}\bar{w} + u_w w_w + u'w')dz$$
$$- (\bar{w}^2 + w_w^2 + w'^2) \tag{9}$$

When Eq. (9) is substituted to Eq. (7) with Assumption -1, we can obtain Eq. (10).

$$\frac{\partial \overline{u}}{\partial t} + \frac{\partial \overline{u}^2}{\partial x} + \frac{\partial \overline{uw}}{\partial z} = -\frac{\partial}{\partial x}\left\{g(\overline{\eta} - z) + \left[\frac{\partial}{\partial t}\int_z^\eta \overline{w}dz + \frac{\partial}{\partial x}\int_z^\eta \overline{uw}dz - \overline{w}^2\right]\right\}$$

$$-\frac{\partial}{\partial x}\left\{g\eta_w + \left[\frac{\partial}{\partial t}\int_z^\eta w_w dz + \frac{\partial}{\partial x}\int_z^\eta u_w w_w dz - w_w^2\right]\right\} - \left\{\frac{\partial u_w}{\partial t} + \frac{\partial u_w^2}{\partial x} + \frac{\partial u_w w_w}{\partial z}\right\}$$

$$-\frac{\partial}{\partial x}\left\{g\eta' + \left[\frac{\partial}{\partial t}\int_z^\eta w' dz + \frac{\partial}{\partial x}\int_z^\eta u'w' dz - w'^2\right]\right\} - \left\{\frac{\partial u'}{\partial t} + \frac{\partial u'^2}{\partial x} + \frac{\partial u'w'}{\partial z}\right\}$$

$$(10)$$

After averaging the Eq. (10) over a wave period, Eq. (11) is finally obtained.

$$\left(\frac{\partial \overline{u}}{\partial t} + \right)\frac{\partial \overline{u}^2}{\partial x} + \frac{\partial \overline{uw}}{\partial z} = -\frac{\partial}{\partial x}\left\{g(\overline{\eta} - z) + \frac{1}{T}\int_0^T\left[\frac{\partial}{\partial x}\int_z^\eta \overline{uw}dz - \overline{w}^2\right]dt\right\}$$

$$-\frac{1}{T}\int_0^T\left[\frac{\partial}{\partial x}\left\{g\eta_w + (u_w^2 - w_w^2) + \frac{\partial}{\partial x}\int_z^\eta u_w w_w dz\right\} - \left\{\frac{\partial u_w w_w}{\partial z}\right\}\right]dt \quad (11)$$

$$-\frac{1}{T}\int_0^T\left[\frac{\partial}{\partial x}\left\{g\eta' + (u'^2 - w'^2) + \frac{\partial}{\partial x}\int_z^\eta u'w' dz\right\} - \left\{\frac{\partial u'w'}{\partial z}\right\}\right]dt$$

Here some assumptions are added; the wave components are expressed by small amplitude wave theory (Assumption-2), third-order terms of wave height are sufficiently small and can be neglected (Assumption-3), the gradient of the Reynolds stress in the horizontal direction is much smaller than that of radiation stress based on the Stive et al. (1982) (Assumption-4) and the vertical acceleration of time-mean component is small (Assumption-5). Adding these assumptions, the Eq. (11) for the momentum conservation of the time-mean components becomes the following equation.
From the still water level to the bottom $(-h \leq z \leq 0)$,

$$\left(\frac{\partial \overline{u}}{\partial t} + \right)\frac{\partial \overline{u}^2}{\partial x} + \frac{\partial \overline{uw}}{\partial z} = -\frac{\partial}{\partial x}g(\overline{\eta} - z) - \frac{\partial}{\partial x}(\overline{u}_w^2 - \overline{w}_w^2) - \frac{\partial \overline{u'w'}}{\partial z} \quad (12)$$

and, for above the still water level $(0 \leq z \leq \eta)$,

$$\left(\frac{\partial \overline{u}}{\partial t} + \right)\frac{\partial \overline{u}^2}{\partial x} + \frac{\partial \overline{uw}}{\partial z} = -\frac{\partial}{\partial x}g(\overline{\eta} - z) - \frac{1}{T}\int_0^T\frac{\partial}{\partial x}g\eta_w\, dt - \frac{\partial \overline{u'w'}}{\partial z} \quad (13)$$

Equation (12) and (13) consist of four terms; acceleration, hydrostatic pressure, radiation stress and the Reynolds stress terms.

The continuity equation (1) becomes Eq.(14) by following the similar process.

$$\frac{\partial \overline{u}}{\partial x} + \frac{\partial \overline{w}}{\partial z} = 0 \tag{14}$$

The water depth is divided into an appropriate number of the horizontal layers. The sketch of layer is shown in Fig. 1. The layer are numbered from top to bottom. The h_i indicates the depth at the lower boundary of the number i th layer. The surface of the first layer is the mean water level $\overline{\eta}$ and the lowest boundary is the bottom surface.
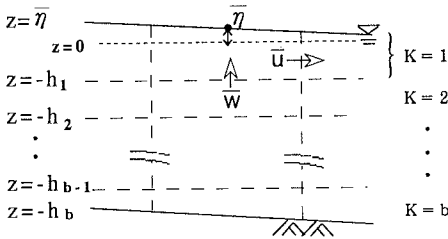
Figure-1   Lay-out of Multi-Layer

In order to obtained the governing equations for each layer, Eq. (12), (13) and (14) are integrated between the upper and lower boundary of each layer with an assumption that the time-mean horizontal velocity $\overline{u}$ is constant in each layer (Assumption-6).

<u>Momentum Equation</u>
The Top Layer (k=1)

$$\frac{\partial \overline{P_1}}{\partial t} + \frac{\partial \overline{P_1 u_1}}{\partial x} - \overline{u_1} \overline{w_1}\Big|_{z=-h1}$$

$$= -g\left(\overline{\eta} - (-h_1)\right) \frac{\partial \overline{\eta}}{\partial x} - \frac{\partial}{\partial x}\left(\frac{1}{2}\overline{\eta^2} + \int_{h1}^{0}\left(\overline{u_w^2} - \overline{w_w^2}\right)dz\right) - \overline{u'w'}\Big|_{z=-h1}$$

$$\tag{15}$$

The Middle Layer (k= i)

$$\frac{\partial \overline{P_i}}{\partial t} + \frac{\partial \overline{P_i u_i}}{\partial x} + \overline{u_i}\overline{w_i}\Big|_{z=-hi-1} - \overline{u_i}\overline{w_i}\Big|_{z=-hi}$$

$$= -g\left((-h_{i-1}) - (-h_i)\right)\frac{\partial \overline{\eta}}{\partial x} - \frac{\partial}{\partial x}\left(\int_{-hi}^{-hi-1}\left(\overline{u_w^2} - \overline{w_w^2}\right)dz\right) + \overline{u'w'}\Big|_{z=hi-1} - \overline{u'w'}\Big|_{z=-hi}$$

$$\tag{16}$$

The Bottom Layer (k= b)

$$\frac{\partial \overline{P}_b}{\partial t} + \frac{\partial \overline{P}_b \overline{u}_b}{\partial x} + \overline{u}_b \overline{w}_b\big|_{z=-hb-1}$$
$$= -g\big((-h_{b-1}) - (-h_b)\big)\frac{\partial \overline{\eta}}{\partial x} - \frac{\partial}{\partial x}\left(\int_{hb}^{-hb-1}\left(\overline{u_w^2} - \overline{w_w^2}\right)dz\right) + \overline{u'w'}\big|_{z=-hb}$$

$$(17)$$

<u>≤Continuity Equation></u>
The Top Layer (k=1)

$$\left(\frac{\partial \overline{\eta}}{\partial t}\right) + \frac{\partial \overline{P}_1}{\partial x} - \overline{w}_1 = 0 \tag{18}$$

The Middle Layer (k= i)

$$\frac{\partial \overline{P}_1}{\partial x} + \overline{w}_{i-1} - \overline{w}_i = 0 \tag{19}$$

The Bottom Layer (k= b)

$$\frac{\partial \overline{P}_b}{\partial x} + \overline{w}_b = 0 \tag{20}$$

where,

$$\overline{P}_i \equiv \int_{-h_i}^{-h_{i-1}} u_i dz \tag{21}$$

The governing equations in the present model are from Eq. (15) to (20). A bottom friction term is added to Eq. (17).

These governing equations are solved numerically with a modified ADI method (Maa, 1990; Sato et al., 1992). The variables to be obtained are time-mean velocity $\overline{u}$, $\overline{w}$ in each layer and time-mean water level $\widetilde{\eta}$ at the top layer. The radiation stress in each layer is calculated using water particle velocities and water surface elevation calculated by the small amplitude wave theory. The total amount of this stress over the water depth is the same as the conventional radiation stress introduced by Lounguet-Higgins et al.(1964). The Reynolds stresses are represented by the eddy viscosity model. The eddy viscosity coefficients are estimated by the empirical formula introduced by Okayasu et al. (1988), for the onshore area between plunging point and shoreline. For the area off the breaking point, this coefficient is set to be zero. In the area between plunging and breaking points, the coefficient is calculated by linear interpolation. The bottom friction is expressed with a term proportional to the square of time-mean velocity.

3. Theoretical Consideration on the Present Model

As waves approach to the shore, a part of the momentum of wave motion is transferred to a flow. Since the total momentum of water motion in the surf zone is conserved, changes in wave momentum in the horizontal direction should balance with the momentum of time-mean currents. This phenomenon is expressed in the Navie-Stokes momentum equations. Equation (22) is the Navier-Stokes equation expressed by the time-mean and wave components, and is same as Eq. (10) excluding the turbulent term.

$$\frac{\partial \overline{u}}{\partial t} + \frac{\partial \overline{u}^2}{\partial x} + \frac{\partial \overline{uw}}{\partial z} + \frac{1}{\rho}\frac{\partial \overline{p}}{\partial x} = -\left(\frac{\partial u_w}{\partial t} + \frac{\partial u_w^2}{\partial x} + \frac{\partial u_w w_w}{\partial z} + \frac{1}{\rho}\frac{\partial p_w}{\partial x} \right) \qquad (22)$$

The left side shows the balance of the time-mean component while the right side is for the wave component. If the wave momentum decreases, the momentum of flow must increase for conserving the total momentum. The transferred momentum in an averaged wave period is expressed as the difference in the radiation stresses.

When a wave breaks and jet and large vortexes occur, the momentum of jet and vortexes must be supplied from the wave motion. The source of the time-mean momentum of the vortex is also the difference in the radiation stress. In the models for the vertical circulation, the vortex is often dealt as outer source of force to the time-mean flow (e.g. Péchon et al., 1994). However, from the above-mentioned consideration, it is sufficient to take only change in the radiation stress as driving force of the time-mean flow. This is the basic concept of this model.

As the radiation stress is dealt with as an integrated form over a water depth until now, we can not take into consideration its vertical distribution. However, it is needed to express the strong transfer by wave breaking around the water surface. Figure-2(a) shows an example of calculated result for the gradient of radiation stress after wave breaking. The gradient around the surface is the steepest throughout the depth. This result expresses that the momentum is transferred from wave to large vortexes in a wave period. Figure-2(b) shows hydrostatic time-mean pressure at the same point. Comparing the pressure force and radiation stresses, onshore force induced
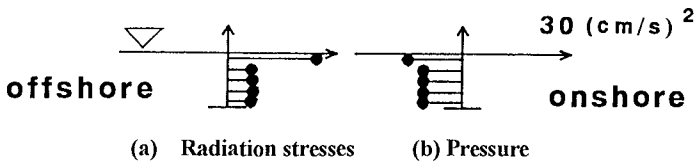
(a)   Radiation stresses   (b) Pressure
Figure-2   Imbalance of radiation stresses and hydrostatic pressure

by the radiation stress is stronger than offshore pressure force at the top layer. On the other hand, they are opposite in other layers i.e.; offshore force induced by pressure is stronger. This means that the present model can represent the vertical distribution of driving forces and their local imbalance.

These local imbalances of radiation stress and time-mean hydrostatic pressure force indicate how the vertical circulation is generated. The distribution of time-mean water level which causes the gradient of hydrostatic pressure force can be explained by the radiation stress. Then, we can explain the generation of the vertical circulation with radiation stresses as a source of driving force.

4. Comparisons of Results between Simulations and Experiments.

The present model was applied to predict time-mean water level and vertical distribution of on- and off-shore time-mean currents. The following three experiments were chosen for the comparison.

(Case-a) Vertical Circulation and Wave Set-up/Set-down in Wave Flume (2-DV)

In this case, the experiments were divided two sorts. First one was designed to compare the distribution of mean water level and pattern of vertical circulation in a surf zone. The wave flume was 20 m long and 0.6 m wide with a beach of 1/20 slope. The water depth in the uniform area was 35 cm. Two different wave conditions were used; spilling breaker (Case-a-1) and plunging breaker (Case-a-2). Surface elevations and velocity were measured by capacitance-type wave gauge and electromagnetic current meter respectively.

The other experiment was performed by Okayasu et al.(1988), in which vertical distribution of cross-shore current was measured in detail by laser-Doppler velocimeter. The wave flume was 23 m long and 0.4m wide with a 1/20 slope. Water depth in the uniform area is 40 cm. Six lines were chosen to measure the currents. Line-1 is at the breaking point and Line-6 is on the still water shore line. Two conditions of incident wave were chosen; plunging breaker (Case-a-3) and spilling breaker (Case-a-4).

(Case-b) Weak Three-Dimensional Nearshore Currents in Wave Basin

This case was chosen to check the capacity of this model to predict the vertical distribution of long- and cross-shore currents. This experiment was performed by Okayasu et al.(1994), and the currents observed in the experiments was not strong. The condition of the experiment and simulation are shown in Fig.-3. The wave basin has a 1/20 uniform slope which is uniform in the long-shore direction. Wave enters at an angle of 10 degree to cross-shore line.
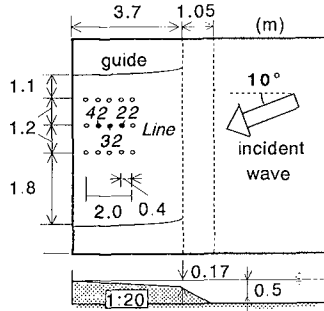
Figure-3 Top and Side View of Wave basin (Case-b)
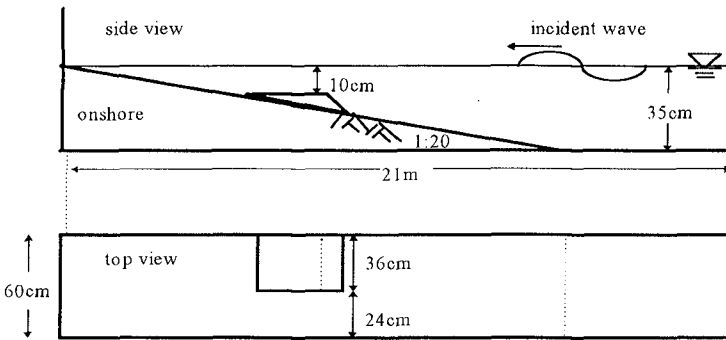
Figure-4 Wave flume with a step (Case-c)

(Case-c) Strong Three-Dimensional Nearshore Currents Around a Step

This case was selected to examine the capacity to predict the three-dimensional nearshore fast currents. Figure-4 shows a schematic diagram of the wave fume. The width of the step were three fifth of the flume width in order to cause three-dimensional currents.

Table-1 shows the conditions of these cases, where Hi and T are height and period of incident waves, and h is the water depth in the offshore.

Table-1   Experimental Condition

	Incident Wave			Breaking Type	Experiment
	Hi (cm)	T (s)	h (cm)		
Case-a-1	10.0	1.0	35	spilling	Present study
Case-a-2	12.0	2.0	35	plunging	Present study
Case-a-3	8.5	2.0	40	plunging	Okayasu (1988)
Case-a-4	9.87	1.17	40	spilling	Okayasu (1988)
Case-b	5.5	1.33	49.7		Okayasu (1994)
Case-c	7.5	1.75	35	plunging	Present study

(1) Results of Vertical Circulation and Wave Set-up/Set-down (Case-a)

Figure-5(a) and 5(b) show the results of Case-a-1 and Case-a-2 respectively. The line and marks in each figure indicate the mean-water level obtained by the simulation and experiment respectively. Both results of the simulation show good agreement with the experimental results, though wave set-down are slightly overestimated around the wave breaking point. Simulated and measured cross-shore currents are shown by arrows with solid line and broken line respectively. The direction of vertical circulation of both simulated results is onshore at the uppermost level and offshore below the second level which is nearly equal to wave trough level. These patterns correspond to the experimental results.
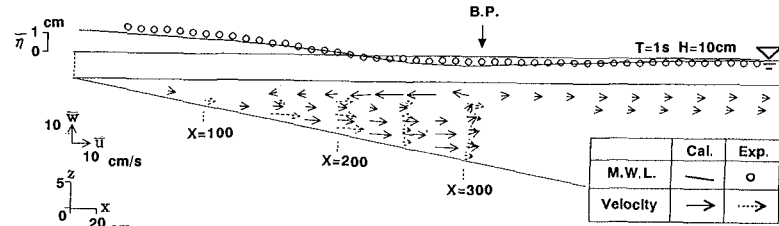
(a) Case-a-1 (Spilling breaking type)
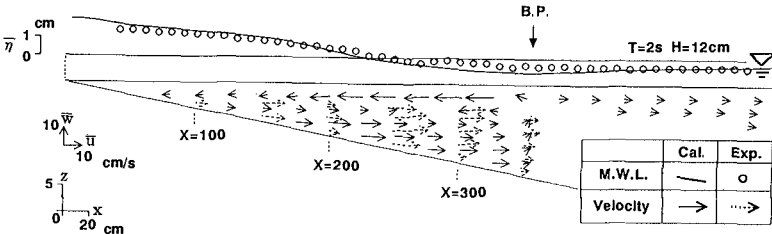
(b) Case-a-2 (Plunging breaking type)

Figure-5 Vertical Circulation and Wave Set-up/Set-down (Case-a)

| Line - 1 | Line - 2 | Line - 3 | Line - 4 | Line - 5 | Line - 6 |

10cm/s

offshore   onshore

(a) Case-a-3 (Plunging breaking type)

--- exp.
•— cal.

(b) Case-a-4 (Spilling breaking type)
Figure-6 Vertical Distribution of cross-shore current(Case-a)
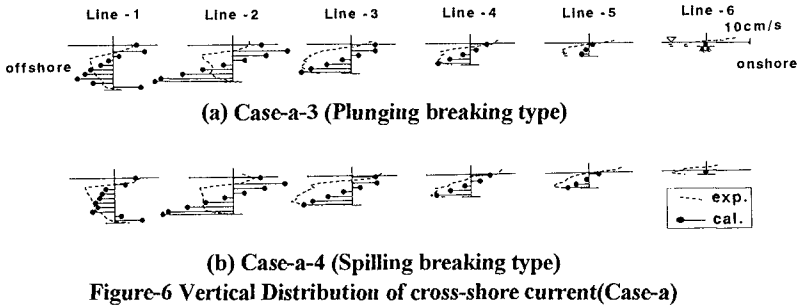
The calculated results and experimental data measured by laser-Doppler velocimeter are compared in Figure-6(a) and 6(b) in order to examine the vertical distribution of cross-shore current in detail. Simulation results are indicated by filled circles with line and experimental results are by broken lines. From Line-3 to Line-5, where large vortexes progress, simulated vertical distribution show good agreement with experiments. On the other hand, the agreement is not so good at Line-2 and 6, which are near the breaking point and the shore line, respectively.

(2) Results of Weak 3-D Currents (Case-b)

It is important to properly predict time-mean water level, since the gradient of the water level is one of the driving force of currents. Figure-7 shows the comparison for the water level. The results by the present multi-layer model and single layer model which have been used conventionally are indicated by a circle and a triangle respectively. The results of both simulations are in close agreement with that of experiments.

Figure-8(a) shows the vertical distribution of currents simulated simultaneously with the water level. The vertical axis shows the water depth. The horizontal axes show the cross- and long-shore directions. The solid lines show the calculated cross- and long-
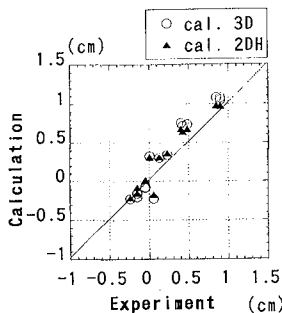
Figure-7   Wave Set-up/Set-down

shore current velocities, and the solid lines with filled circle show the sum of these velocities. On the other hand, the broken lines show the measured currents.

In both results of simulation and experiment, cross-shore currents are onshore above the wave trough level and offshore under the trough level. In the long-shore direction, there is a vertical distribution of the current velocity i.e.; it is slow near the surface, fast in the middle, and slow again near the bottom. The simulated currents velocities agree approximately with experiments in the area where the water depth is a comparatively large as Line-22. On the other hand, in the area where the depth is small as Line-42, the simulated velocities are far slower than experiment. This reason may be that the present model can not yet express the distribution of radiation stress well in the shallow region.

Next, the present multi-layer model is compared with a single layer model which have been used conventionally. For the result of single layer model (Fig.-8(b)), cross-shore current dose not appear and long shore currents are of course uniform over the depth. Such comparison shows the effectiveness of the multi-layer model for the simulation of the three-dimensional structure of the nearshore currents.
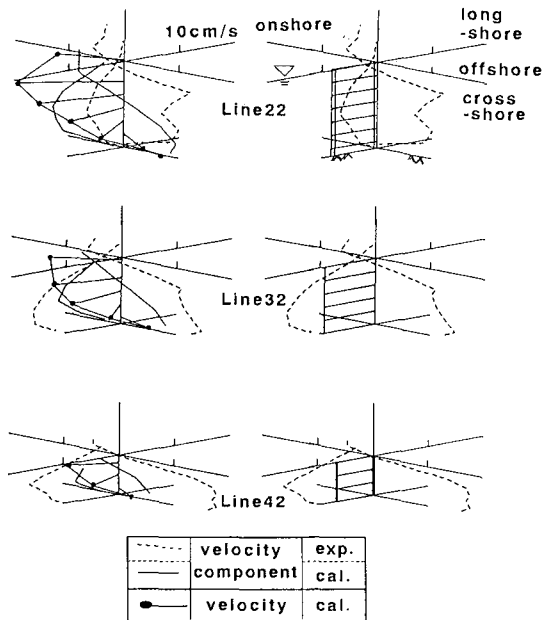
(a)Multi-Layer Model   (b) Single-Layer model

Figure-8   Vertical Distribution of Cross- and Long-Shore Currents (Case-b)

(a) Numerical Simulation
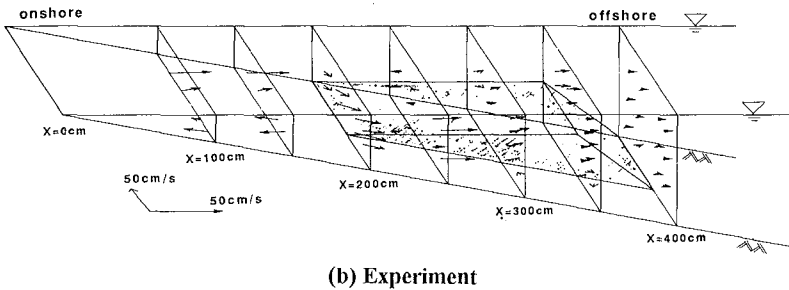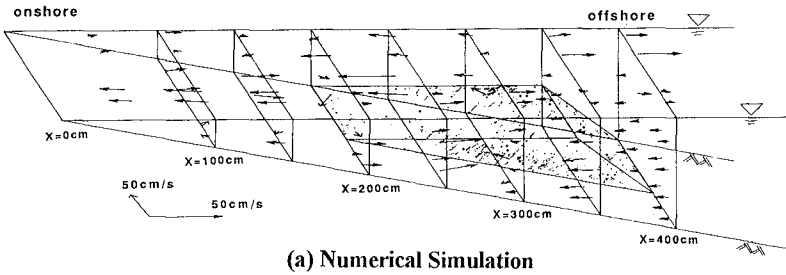
(b) Experiment
Figure-9 Three-dimensional currents around the step (Case-c)

(3) Results of Strong 3-D Currents (Case-c)

Figure-9(a) and (b) show the simulated and measured results of the near-shore currents around the step. The currents were measured only under wave trough by a electromagnetic current meter. In the results of simulation, there are circulations around the step and near the shore line respectively. The circulation around the step is anti-clockwise; i.e., it directs onshore above the step and offshore at the gap of structure. The other circulation show the reverse rotation. Detailed examination of simulated results shows that flow moves from one to another circulation and vice versa.   Part of streamlines forms a "8" shape with a two-level crossing. The measured and observed result showed a similar pattern of circulation.

Another remarkable three-dimensional structure is that offshore currents near the bottom of the gap turn to a rising current a long the step in the vicinity of $x=300$ line. This pattern of current is also reproduced in the simulation.

5. Conclusion

In this study, a three-dimensional nearshore current model based on the vertical distribution of the radiation stresses was developed. As the driving force of this model is only radiation stresses, it is comparatively easy to calculate the time mean flow for the

three-dimensional beach. Simulated results for wave set-up/set-down and vertical distribution of cross- and long-shore currents show good agreement with measured data. The above results confirm that this model is effective to estimate three-dimensional nearshore current in the surf zone.

Acknowledgments

Reference

Dyhr-Nielsen M. and T. Sørensen.(1970): Some sand transport phenomena on coast with bars, Proc. 12th. ICCE, pp.855-865.

Longuet-Higgins M. S. and R. W. Stewart (1964): Radiation stresses in water waves ; a physical discussion, with applications, Deep-sea Res.11, pp.529-562.

Maa J. P.-Y.(1990): An efficient horizontal two-dimensional hydrodynamic model, Coastal Engineering, vol.14, pp.1-18.

Okayasu A., T. Shibayama and K. Horikawa (1988) Vertical variation of undertow in the surf zone, Proc. 21st. ICCE, pp.478-491.

Okayasu A., K. Hara and T. Shibayama (1994): Laboratory experiments on 3-D nearshore current and a model with momentum flux by breaking waves, Proc. 24th. ICCE, pp.2461-2475.

Péchon P. and C. Tesson (1994) : Numerical modeling of three-dimensional wave-induced currents in the surf zone, Proc.24th. ICCE, pp.2503-2512.

Sato S. and K. Ueda (1992): Numerical simulation of tide and wind induced currents in Tokyo Bay, JSCE, Vol. 39(1), pp.251-255, (in Japanese).

Stive M. J. F. and H. G. Wind (1982): A study of radiation stress and set-up in the nearshore region, Coastal Engineering, vol.6, pp.1-25.

Svendsen I. A.(1984): Mass flux and undertow in a surf zone, Coastal Engineering, Vol.8, pp.347-365.

Svendsen I. A. and R. Lorenz (1988): Velocities in combined undertow and longshore currents, Coastal Engineering, Vol.13, pp.55-79.